

Perturbative approach to the structure of rapidly rotating neutron stars

Omar Benhar^{1,2}, Valeria Ferrari^{1,2}, Leonardo Gualtieri^{1,2}, Stefania Marassi¹

¹ *Dipartimento di Fisica “G. Marconi”, Università degli Studi di Roma, “La Sapienza”, P.le A. Moro 2, 00185 Roma, Italy*

² *INFN, Sezione Roma 1, P.le A. Moro 2, 00185 Roma, Italy*

(Dated: October 1, 2018)

We construct models of rotating stars using the perturbative approach introduced by J. Hartle in 1967, and a set of equations of state proposed to model hadronic interactions in the inner core of neutron stars. We integrate the equations of stellar structure to third order in the angular velocity and show, comparing our results to those obtained with fully non linear codes, to what extent third order corrections are needed to accurately reproduce the moment of inertia of a star which rotates at rates comparable to that of the fastest isolated pulsars.

PACS numbers: PACS numbers: 04.40.Dg, 97.60.Jd, 26.60+c

I. INTRODUCTION

In this paper we show that the structure of a rapidly rotating neutron star can be described to a high level of accuracy by using the perturbative approach introduced by Hartle in 1967 [1], subsequently developed to third order in the angular velocity Ω [2].

There are several reasons why the perturbative approach may be preferred to the direct numerical integration of Einstein’s equations for stellar structure. One is that the angular behaviour of the solution is given explicitly in terms of Legendre polynomials of first kind, whereas the radial behaviour can be found by integrating linear differential equations in the radial variable; thus, instead of solving the nonlinear, coupled, partial differential equations of the exact theory one simply integrates a set of ordinary, linear differential equations. Moreover, these equations need to be integrated only inside the star, because the exterior solution can be found explicitly in terms of known polynomials. A further element of interest is that the perturbative approach allows to evaluate to what extent a physical quantity changes at each order in Ω , and to check whether the n^{th} -order contribution is needed to estimate a chosen quantity or whether the first order estimates, often used to interpret astronomical observations, are enough. For these reasons, the perturbative approach expanded to 2nd order in rotation rate has been used by several authors to study properties of rotating neutron stars [3, 4, 5, 6, 7, 8, 9] (see also the review [10] and refereces therein).

On the other hand the perturbative approach has a drawback, since it fails when the angular velocity approaches the mass-shedding limit, i.e. when the star rotates so fastly that the gravitational attraction is not sufficient to keep matter bound to the surface; numerical integration of the exact equations shows that in these conditions a cusp forms on the equatorial plane of the star [11, 12, 13], which cannot be reproduced by the first few orders of the perturbative expansions (we shall discuss this point quantitatively in section III). However, the rotation rate of all known pulsars is much lower than the mass-shedding limit for most equations of state (EOS)

considered in the literature. Thus, unless we are specifically interested in the mass-shedding problem, we can use the perturbative approach to study the structural properties of the observed neutron stars. The problem is to establish how many terms in the expansion we need to consider to describe, say, the fastest isolated pulsar observed so far, PSR 1937+21, whose period is $T = 1.56$ ms, and this is the question we plan to answer in this paper. The equations of structure for uniformly rotating stars have been developed to second order in the angular velocity in [1, 3] and subsequently extended to third order in [2]. With respect to the derivation of [2] we introduce two novelties:

- the third order corrections involve two functions, w_1 and w_3 . w_1 gives a contribution to the moment of inertia, w_3 affects the mass-shedding velocity. Both w_1 and w_3 , contribute to the dragging of inertial frames. In [2] the solution for w_1 was given explicitly outside the star in terms of Legendre polynomials of second kind; that expression contained some errors that we correct. In addition, we complete the third order solution giving the explicit expression of w_3 outside the star.

- In [2] a procedure was developed to construct families of constant baryonic mass solutions with varying angular velocity, which was applied to study the behaviour of the moment of inertia along such sequencies, for small values of the angular velocities. This procedure cannot be applied to fastly rotating stars and furthermore, it was shown to be unstable when the stellar mass approaches the maximum mass for any assigned equation of state. In this paper we develop, and apply, a different algorithm that allows to describe a sequence of constant baryonic mass stars at any value of the angular velocity (smaller than the mass-shedding limit), and which is stable also in the maximum mass limit.

In section II we shall briefly explain what are the corrections to the metric and to the thermodynamical functions that are needed to describe the structure of a rotating star to third order in Ω , and in the appendix we shall summarize the equations they satisfy inside and outside the star.

In order to test the perturbative scheme, we shall com-

pare the results we find solving these equations for three selected EOS, with those of ref. [13] and [14] where the exact Einstein equations have been integrated for the same EOS. To hereafter, the adjective “exact” referred to Einstein’s equations will mean that the full set of equations is solved numerically and non-perturbatively. This comparison will be discussed in section III and will allow us to assess the validity of the third order approach.

We shall then integrate the third order equations to model a neutron star composed of an outer crust, an inner crust and a core, each shell being described by a non viscous fluid which obeys equations of state appropriate to describe different density regions. There is a general consensus on the matter composition of the crust, for which we use two well established EOS: the Baym-Pethick-Sutherland (BPS) EOS [15] for the outer crust ($10^7 \lesssim \rho \lesssim 4 \cdot 10^{11}$ g/cm³), and the Pethick-Ravenhall-Lorenz (PRL) EOS [16] for the inner crust ($4 \cdot 10^{11} \lesssim \rho \lesssim 2 \cdot 10^{14}$ g/cm³).

For the inner core, $\rho > 2 \cdot 10^{14}$ g/cm³, we use recent EOS which model hadronic interactions in different ways leading to different composition and dynamics. The main assumptions underlying these EOS will be outlined in section IV.

For a given EOS there are two kind of equilibrium configurations, ususally indicated as ”normal” and ”supramassive”. They both refer to rotating stars with constant baryonic mass and varying angular velocity. Each normal sequence has, as a limiting configuration, a non rotating, spherical star. The supramassive sequences do not possess this limit, and all members of a sequence have a baryonic mass larger than the maximum mass of a non rotating, spherical star. Our study is confined to stars belonging to the normal sequence.

The results of our calculations will be discussed in section V.

II. THE METRIC AND THE STRUCTURE OF A ROTATING STAR

In this section we introduce all the quantities that describe the star to third order in the angular velocity Ω . Following [1, 2, 3] we write the metric as

$$ds^2 = -e^{\nu(r)} [1 + 2h(r, \theta)] dt^2 + e^{\lambda(r)} \left[1 + \frac{2m(r, \theta)}{[r - 2M(r)]} \right] dr^2 + r^2 [1 + 2k(r, \theta)] \{ d\theta^2 + \sin^2 \theta [d\phi - w(r, \theta)dt]^2 \}. \quad (1)$$

Here $e^{\nu(r)}$, $e^{\lambda(r)}$ and $M(r)$ are functions of r and describe the non rotating star solution of the TOV equations (see Appendix A). The functions $h(r, \theta)$, $m(r, \theta)$, $k(r, \theta)$ and

$w(r, \theta)$ are the perturbative corrections

$$h(r, \theta) = h_0(r) + h_2(r)P_2(\theta) + O(\Omega^4) \quad (2)$$

$$m(r, \theta) = m_0(r) + m_2(r)P_2(\theta) + O(\Omega^4) \quad (3)$$

$$k(r, \theta) = k_2(r)P_2(\theta) \quad (4)$$

$$= [v_2(r) - h_2(r)] P_2(\theta) + O(\Omega^4)$$

$$w(r, \theta) = \omega(r) + w_1(r) \quad (5)$$

$$- w_3(r) \frac{1}{\sin \theta} \frac{dP_3(\theta)}{d\theta} + O(\Omega^5)$$

$P_2(\theta)$ and $P_3(\theta)$ are the $l = 2$ and $l = 3$ Legendre polynomials. As described in [1, 2, 3], the function ω is of order Ω , whereas $(h_0, h_2, m_0, m_2, k_2, v_2)$ are of order Ω^2 , and (w_1, w_3) are of order Ω^3 . In a similar way, the displacement that an element of fluid, located at a given (r, θ) in the non rotating star, experiences because of rotation can be expanded in even powers of Ω

$$\xi = \xi_0(r) + \xi_2(r)P_2(\theta) + O(\Omega^4), \quad (6)$$

where both $\xi_0(r)$ and $\xi_2(r)$ are of order Ω^2 . We shall assume that matter in the star is described by a perfect fluid with energy momentum tensor

$$T^{\mu\nu} = (\epsilon + P)u^\mu u^\nu + P g^{\mu\nu}. \quad (7)$$

Since the fluid element is displaced, its energy density and pressure change; in a reference frame that is momentarily moving with the fluid, the pressure variation is

$$\delta P(r, \theta) = [\epsilon(r) + P(r)] [\delta p_0(r) + \delta p_2(r)P_2(\theta)] \quad (8)$$

and it can be expressed in terms of ξ as follows

$$\delta p_0(r) = -\xi_0(r) \left[\frac{1}{\epsilon + P} \frac{dP}{dr} \right], \quad (9)$$

$$\delta p_2(r) = -\xi_2(r) \left[\frac{1}{\epsilon + P} \frac{dP}{dr} \right], \quad (10)$$

where $\epsilon(r)$ and $P(r)$ are the energy density and the pressure computed for the non rotating configuration. The corresponding energy density variation of the fluid element is

$$\delta \epsilon(r, \theta) = \frac{d\epsilon}{dP} (\epsilon + P) [\delta p_0(r) + \delta p_2(r)P_2(\theta)]. \quad (11)$$

This last equation has been derived on the assumption that the matter satisfies a barotropic EOS.

In appendix A we shall write the equations satisfied by the corrections to the metric functions and to the thermodynamical variables to the various order in Ω , with the appropriate boundary conditions. It should be stressed that these equations have to be numerically integrated only for $r \leq R$, where R is the radius of the non rotating star. For $r > R$ the solution can be found analytically. Hereafter, $r = R$ and $M(R)$ will indicate, respectively, the radius and the mass of the non rotating star, found by solving the TOV equations for an assigned EOS.

Once the various functions have been computed as shown in Appendix A, we can evaluate how the star changes in shape due to rotation, the moment of inertia, the mass-shedding limit and all quantities one is interested in. Here we shall briefly summarize what are the relevant physical quantities we shall consider.

- *Stellar deformation*

The effect of rotation described by the metric (1) on the shape of the star can be divided in two contributions:

A) A spherical expansion which changes the radius of the star, and is described by the functions h_0 and m_0 .

B) A quadrupole deformation, described by the functions h_2 , v_2 and m_2 .

As a consequence of these two contributions, that are both of order Ω^2 and that will be indicated with the labels A and B, respectively, the radius of the star, the eccentricity and the gravitational mass change as follows.

A fluid element on the surface of the spherical non rotating star, i.e. at $(r = R, \theta)$, will be displaced by an amount δR given by

$$\delta R = \delta R^A + \delta R^B = \xi_0(R) + \xi_2(R)P_2(\theta) \quad (12)$$

where $\xi_0(R)$ and $\xi_2(R)$ can be computed by eqs. (A16) and (A26) as shown in appendix A.

Once we know δR we can compute, for instance the eccentricity of the star

$$E_c = \left[(\text{equatorial radius})^2 / (\text{polar radius})^2 - 1 \right]^{1/2}. \quad (13)$$

The change in the gravitational mass is given by

$$\delta M_{grav} = \left[m_0(R) + \frac{J^2}{R^3} \right]. \quad (14)$$

Notice that δM_{grav} does not depend on quadrupolar perturbations (h_2, v_2, m_2) , nor on the perturbations that are first (ω) and third order (w_1, w_3) in Ω . The reason is that such quantity is invariant under rotations of the system, and it is even for parity transformations (which change $\Omega \rightarrow -\Omega$).

- *Dragging of inertial frames*

The function $\omega(r, \theta)$ in the metric (1) is responsible for the dragging of inertial frames. It affects two important physical quantities, i.e. the mass-shedding limit (section II A) and the moment of inertia (section II C).

A. The mass-shedding limit

The mass-shedding velocity can be found using a procedure developed by [17]. Given a star with assigned

baryonic mass which rotates at a given Ω , let us consider an element of fluid which belongs to the star and is located on the surface at the equator; from the metric (1) it is easy to see that it moves with velocity

$$V^{bound} = e^{\frac{\psi(r, \theta) - \beta(r, \theta)}{2}} \left[\Omega - \left(\omega(r) + w_1(r) - \frac{3}{2}w_3(r) \right) \right], \quad (15)$$

where

$$\begin{aligned} e^{\beta(r, \theta)} &= e^{\nu(r)} [1 + 2h(r, \theta)] \\ e^{\psi(r, \theta)} &= r^2 [1 + 2k(r, \theta)] \sin^2 \theta. \end{aligned} \quad (16)$$

In general, the fluid element will not follow a geodesic of metric (1).

Using the geodesic equations we can also compute the velocity of a particle which moves on a circular orbit just outside the equator, in the co-rotating direction

$$\begin{aligned} V^{free} &= \frac{(\omega' + w_1' - \frac{3}{2}w_3')}{\psi'} e^{\frac{\psi - \beta}{2}} \\ &+ \left\{ \frac{\beta'}{\psi'} + \left[\frac{(\omega' + w_1' - \frac{3}{2}w_3')}{\psi'} e^{\frac{\psi - \beta}{2}} \right]^2 \right\}^{1/2}, \end{aligned} \quad (17)$$

where a prime indicates differentiation with respect to r . In general, for an assigned Ω smaller than the mass-shedding limit the two velocities V^{bound} and V^{free} are different, and in particular

$$V^{bound} < V^{free}.$$

When Ω increases, the two velocities converge to the same limit; when this limit is reached the fluid element on the surface will not be bound anymore and the star will start losing matter from the equator. The value of Ω for which $V^{bound} = V^{free}$ is the mass-shedding limit and will be indicated as Ω_{ms} . It should be stressed that V^{bound} and V^{free} are computed at the equatorial radius of the rotating configuration, i.e.

$$R^{rot} = R + \xi_0(R) - \frac{1}{2}\xi_2(R). \quad (18)$$

In order to apply this procedure, we need to construct sequences of stellar models with constant baryonic mass and variable angular velocity.

B. The algorithm to construct a sequence of constant baryonic mass solutions

The baryonic mass of the star is defined as

$$M_{bar} = \int_{t=const} \sqrt{-g} u^t \epsilon_0 d^3x, \quad (19)$$

where g is the determinant of the 4-dimensional metric, d^3x is the volume element on a $t = constant$ hypersurface, and $\epsilon_0(r) = m_N n_{bar}(r)$ is the rest mass-energy

density, not to be confused with the energy density $\epsilon(r)$. Since all known interactions conserve the baryon number, ϵ_0 is a conserved quantity, i.e.

$$(\epsilon_0 u^\mu)_{;\mu} = 0. \quad (20)$$

The expansion of M_{bar} in powers of Ω is

$$M_{bar} = M_{bar}^{(0)} + \delta M_{bar} + O(\Omega^4) \quad (21)$$

where

$$M_{bar}^{(0)} = 4\pi \int_0^R dr \left(1 - \frac{2M(r)}{r}\right)^{-1/2} r^2 \epsilon_0(r) \quad (22)$$

and

$$\begin{aligned} \delta M_{bar} = & 4\pi \int_0^R r^2 dr \left(1 - \frac{2M(r)}{r}\right)^{-1/2} \\ & \cdot \left\{ \left[1 + \frac{m_0(r)}{r - 2M(r)} + \frac{1}{3} r^2 [\Omega - \omega(r)]^2 e^{-\nu(r)} \right] \epsilon_0(r) \right. \\ & \left. + \frac{d\epsilon_0}{dP} (\epsilon + P) \delta p_0(r) \right\}. \end{aligned} \quad (23)$$

In the following we shall briefly compare the procedure developed by Hartle in [2] to construct constant baryonic mass sequences and the procedure we use.

1. Hartle's procedure

1. Given a central energy density $\epsilon(r=0)$ and an assigned EOS, the TOV equations are solved to find the non rotating configuration; the model is identified by a baryonic mass $M_{bar} = \bar{M}$.
2. For an assigned value of the angular velocity Ω the equations of stellar structure are solved to order Ω^2 , imposing that the correction to the pressure, $\delta p_0(r=0)$ is different from zero. The value of $\delta p_0(r=0)$ is then changed until the sought baryonic mass is reached.

2. Our procedure

Our procedure to generate sequences with constant baryonic mass is the following.

1. Same as point 1 of Hartle's procedure.
2. For an assigned value of Ω we solve the equations of stellar structure up to order Ω^3 , for the different values of $\epsilon(r=0)$, by imposing that $\delta p_0(r=0) = 0$. Among these models we select the one with baryonic mass \bar{M} .

If, in addition, we want to compute the mass-shedding velocity, having computed all metric functions for a given Ω we evaluate V^{bound} and V^{free} . If $V^{bound} = V^{free}$ we

have reached the mass-shedding limit and we stop the procedure. If $V^{bound} < V^{free}$ we choose a higher value of Ω and go to point 2. This procedure can be applied to rapidly rotating stars and to models of stars close to the maximum mass.

Hartle's procedure presents a problem when applied to rapidly rotating stars; indeed if the rotation rate is sufficiently high the change in the central energy density $\delta\epsilon(r=0)$ can be so large that treating this change as a perturbation is inappropriate and produces a large error in all quantities. With our approach, instead, this change is treated as a background quantity (we vary $\epsilon(r=0)$), and the results are much more accurate (as can be seen by the comparison with the "exact" integrations of [13],[14] discussed in section III). A second problem arises when the mass of the star is close to the maximum mass (where we mean the maximum mass along a constant Ω sequence). Since $M_{bar} = M_{bar}(\Omega, \epsilon_c)$, where

$$\epsilon_c \equiv \epsilon(r=0) + \delta\epsilon(r=0)$$

it follows that

$$\left. \frac{\partial \epsilon_c}{\partial \Omega} \right|_{M_{bar}} = - \left. \frac{\partial M_{bar}}{\partial \Omega} \right|_{\epsilon_c} / \left. \frac{\partial M_{bar}}{\partial \epsilon_c} \right|_{\Omega}.$$

Since near the maximum mass

$$\left. \frac{\partial M_{bar}}{\partial \epsilon_c} \right|_{\Omega} \rightarrow 0,$$

it follows that

$$\left. \frac{\partial \epsilon_c}{\partial \Omega} \right|_{M_{bar}} \rightarrow \infty.$$

Consequently, since in Hartle's procedure $\epsilon(r=0)$ is kept constant, and $\delta\epsilon(r=0)$ is treated as a perturbation, the procedure fails.

C. The moment of inertia of a rotating star

The angular momentum of an axisymmetric matter distribution rotating about the symmetry axis can be expressed in terms of a conserved four vector, the angular momentum density

$$J^\mu = T^\mu_\nu \xi^\nu_{(\phi)},$$

where $\xi^\nu_{(\phi)}$ is the Killing vector associated to axial symmetry. The conserved total angular momentum J^{tot} can be found by integrating J^μ over any spacelike hypersurface. Given the coordinate system we use, the natural choice is a $t = const$ hypersurface, and since $\xi^\nu_{(\phi)} = \delta^\nu_\phi$

$$J^{tot} = \int_{t=const} \sqrt{-g} J^0 d^3x = \int_{t=const} \sqrt{-g} T^t_\phi d^3x \quad (24)$$

where, as in (19), g is the determinant of the 4-dimensional metric, and d^3x is the volume element on the chosen hypersurface.

Consequently, the moment of inertia of the matter distribution is

$$I = \frac{J}{\Omega} = \frac{1}{\Omega} \int_{t=const} \sqrt{-g} T^t_\phi d^3x. \quad (25)$$

Using Einstein's equations, in (24) and (25) we can replace T^t_ϕ with $\frac{1}{8\pi} R^t_\phi$ and expand in powers Ω^n . By this procedure it is possible to show that only terms with n odd contribute to this expansion, and that the first terms are

$$J^{tot} = J + \delta J + O(\Omega^5) \quad (26)$$

where J is the first order contribution

$$J = \frac{1}{6} \left[r^4 j(r) \frac{d\varpi}{dr} \right]_{|r=R} \quad (27)$$

and δJ is the third order correction

$$\begin{aligned} \delta J = \frac{1}{6} \left\{ 4r^3 \frac{dj}{dr} \varpi (\xi_0 - \frac{1}{5} \xi_2) + r^4 j \frac{dw_1}{dr} \right. \\ \left. + r^4 j \frac{d\varpi}{dr} \left[h_0 + \frac{m_0}{r-2M} + \frac{4(v_2 - h_2)}{5} \right. \right. \\ \left. \left. - \frac{1}{5} \left(h_2 + \frac{m_2}{r-2M} \right) \right] \right\}_{|r=R}. \quad (28) \end{aligned}$$

In eqs. (27) and (28) the functions ϖ and $j(r)$ are defined as follows

$$\begin{aligned} \varpi(r) &= \Omega - \omega(r), \quad (29) \\ j(r) &= e^{-\nu(r)/2} \sqrt{1 - \frac{2M(r)}{r}}. \end{aligned}$$

Thus, the corrections to the moment of inertia are

$$I = I^{(0)} + \delta I + O(\Omega^4), \quad (30)$$

$$I^{(0)} = \frac{J}{\Omega}, \quad \delta I = \frac{\delta J}{\Omega}. \quad (31)$$

It should be noted that the angular momentum defined in (24) coincides with that defined using the asymptotic behaviour of the metric as in [19] (Ch. 19). In appendix A we shall show how to find δJ from the asymptotic behaviour of the metric function w_1 .

III. A COMPARISON WITH NON-PERTURBATIVE RESULTS

In order to verify to what extent the perturbative scheme correctly describes the physical properties of a rapidly rotating neutron star, we compare the results of the integration of the equations of stellar structure expanded to order Ω^3 with those of ref. [13] and [14], where the fully non linear Einstein equations have been integrated.

To perform the comparison we study stellar sequences with constant baryonic mass and variable spin frequency

$\nu = \Omega/2\pi$, and we choose three EOS labelled as follows: AU - which results from an approach based on nuclear many body theory [20]

APR2 - (APRb in [14]) which takes into account recent results on nuclear many body theory [21, 22]

L - obtained from relativistic mean field theory [23].

AU and L have been used both in [13] and in [14]; the results of the two papers agree to better than 1% for both EOS, except that for the estimate of the moment of inertia for the EOS L, for which the relative error is, at most, of the order of 1.3 %. APR2 has been used in [14] only. Since we interpolate the EOS tables with the same linear interpolation as in [13] (in [14] a 5th-order polynomial has been used), in the following tables our results for AU and L will be compared with those of [13].

For each EOS we consider two stellar sequences with constant baryonic mass and varying angular velocity:

Sequence A, such that the gravitational mass of the non rotating configuration is $M = 1.4 M_\odot$.

Sequence B, that corresponds to the maximum mass.

The corresponding values of the baryonic mass are given in table I.

TABLE I: The baryonic masses of the stellar models used to compare the results of the perturbative approach with those found by integrating the exact Einstein equations are given for the three considered EOS. The data in column 2 and 3 correspond to a non rotating star with gravitational mass $M = 1.4 M_\odot$ and M_{max} , respectively.

	M_{bar}/M_\odot	
AU	1.58	2.64
APR2	1.55	2.69
L	1.52	3.16

The values of ν are chosen as in [13] and [14].

The results of the comparison are summarized in Tables II (sequence A) and III (sequence B), where we show the stellar parameters for different values of the spin frequency. The lines labelled CST and BS refer, respectively, to the data found by integrating the exact equations of stellar structure in [13] and in [14]; BFGM refer to our results found by integrating the equations of stellar structure perturbed to order Ω^3 for the same models and EOS. The spin frequency ν is given in column 2, the central density ϵ_c in column 3, the moment of inertia I in column 4, the gravitational mass M_{grav} in column 5, the equatorial radius R_{eq} in column 6, the ratio between the spin frequency and the mass-shedding frequency (as computed in [13] and [14]) in column 7. For each value of ν and for each quantity, we give the relative error Δ .

We stress that, as explained in Section II, the quantities ϵ_c , M_{grav} and R_{eq} are expanded in powers Ω^n with n even, therefore, as far as our calculations are concerned, they are computed up to order Ω^2 . Conversely, the angular momentum J^{tot} is expanded in odd powers of Ω , and we compute it to order Ω^3 . The moment of inertia I (see eq. 25) is the angular momentum divided by Ω ,

TABLE II: Stellar parameters for the sequence A (see text). Data are computed along a sequence of stellar models with constant baryonic mass corresponding to a non-rotating configuration of mass $M = 1.4 M_{\odot}$ and varying spin frequency $\nu = \Omega/2\pi$ (given in KHz in column 2). ϵ_c is the central density in units of $\epsilon_* = 10^{15} g/cm^3$; the moment of inertia I is in units of $I_* = 10^{45} g cm^2$, the equatorial radius R_{eq} is in km. For each value of ν and for each quantity, we give the relative error Δ . M_{grav} is the gravitational mass in solar mass units. In the last column the ratio of the spin frequency and the mass-shedding frequency (as computed in [13] and [14]) is given.

EOS AU ($M_{bar} = 1.58 M_{\odot}$)						
	ν (KHz)	ϵ_c/ϵ_*	I/I_*	M_{grav}/M_{\odot}	R_{eq} (Km)	ν/ν_{ms}
CST	0	1.206	1.160	1.400	10.40	0
BFGM	0	1.204	1.154	1.395	10.39	
Δ	-	0.2%	0.5%	0.4%	0.1%	
CST	0.476	1.192	1.191	1.403	10.59	0.379
BFGM	0.476	1.190	1.182	1.398	10.56	
Δ	-	0.2%	0.8%	0.4%	0.3%	
CST	0.896	1.148	1.292	1.412	11.22	0.713
BFGM	0.896	1.155	1.254	1.405	11.02	
Δ	-	0.6%	2.9%	0.5%	1.8%	
CST	1.082	1.111	1.386	1.412	11.87	0.861
BFGM	1.082	1.132	1.298	1.410	11.34	
Δ	-	1.9%	6.3%	0.1%	4.5%	
CST	1.257	1.048	1.566	1.432	14.44	1.000
BFGM	1.257	1.108	1.344	1.414	11.73	
Δ	-	5.7%	14.2%	1.3%	18.8%	
EOS APR2 ($M_{bar} = 1.55 M_{\odot}$)						
BS	0	0.995	-	1.403	11.55	0
BFGM	0	0.988	1.310	1.389	11.58	
Δ	-	0.7%	-	1.0%	0.3%	
BS	0.554	0.970	1.396	1.409	11.99	0.532
BFGM	0.554	0.964	1.373	1.394	11.97	
Δ	-	0.6%	1.6%	1.0%	0.2%	
BS	0.644	0.960	1.425	1.411	12.18	0.619
BFGM	0.644	0.956	1.395	1.396	12.12	
Δ	-	0.4%	2.1%	1.0%	0.5%	
BS	0.879	0.920	1.551	1.418	13.05	0.844
BFGM	0.879	0.929	1.466	1.401	12.63	
Δ	-	1.0%	5.5%	1.2%	3.2%	
BS	1.041	0.870	1.737	1.428	15.04	1.000
BFGM	1.041	0.905	1.526	1.405	13.13	
Δ	-	4.0%	12.1%	1.6%	13.0%	
EOS L ($M_{bar} = 1.52 M_{\odot}$)						
CST	0	0.433	2.127	1.400	14.99	0
BFGM	0	0.440	2.120	1.402	14.99	
Δ	-	1.6%	0.3%	0.1%	0.0%	
CST	0.283	0.427	2.194	1.402	15.30	0.395
BFGM	0.283	0.433	2.182	1.404	15.27	
Δ	-	1.4%	0.5%	0.1%	0.2%	
CST	0.505	0.411	2.378	1.407	16.22	0.705
BFGM	0.505	0.419	2.307	1.408	15.95	
Δ	-	1.9%	3.0%	0.1%	1.7%	
CST	0.609	0.398	2.548	1.412	17.17	0.851
BFGM	0.609	0.410	2.385	1.410	16.43	
Δ	-	3.0%	6.4%	0.1%	4.3%	
CST	0.716	0.377	2.881	1.419	21.25	1.000
BFGM	0.716	0.400	2.473	1.414	17.06	
Δ	-	6.1%	14.2%	0.4%	19.7%	

TABLE III: The stellar parameters for the sequence B, corresponding to the maximum mass (see text) are given as in table II.

EOS AU ($M_{bar} = 2.64 M_{\odot}$)						
	ν (KHz)	ϵ_c/ϵ_*	I/I_*	M_{grav}/M_{\odot}	R_{eq} (Km)	ν/ν_{ms}
CST	0	3.020	1.982	2.133	9.41	0
NOI	0	3.020	1.964	2.126	9.39	
Δ	-	0.0%	0.9%	0.3%	0.2%	
CST	0.602	2.547	2.077	2.141	9.74	0.357
NOI	0.602	2.566	2.058	2.135	9.71	
Δ	-	0.7%	0.9%	0.3%	0.3%	
CST	1.174	2.101	2.281	2.170	10.40	0.697
NOI	1.174	2.159	2.218	2.158	10.19	
Δ	-	2.8%	2.8%	0.6%	2.0%	
CST	1.481	1.813	2.525	2.201	11.20	0.879
NOI	1.481	1.968	2.344	2.178	10.58	
Δ	-	8.5%	7.2%	1.0%	6.0%	
CST	1.625	1.637	2.766	2.227	12.10	0.964
NOI	1.625	1.881	2.416	2.187	10.82	
Δ	-	15.0%	12.7%	1.8%	10.6%	
CST	1.684	1.532	2.974	2.246	13.66	1.000
NOI	1.684	1.844	2.448	2.192	10.93	
Δ	-	20.0%	17.7%	2.4%	20.0%	
EOS APR2 ($M_{bar} = 2.69 M_{\odot}$)						
BS	0	2.600	-	2.205	10.12	0
BFGM	0	2.748	2.219	2.202	10.03	
Δ	-	5.7%	-	0.1%	0.9%	
BS	0.609	2.300	2.352	2.217	10.45	0.408
BFGM	0.609	2.292	2.347	2.212	10.44	
Δ	-	0.3%	0.2%	0.2%	0.1%	
BS	1.081	1.900	2.593	2.243	11.21	0.723
BFGM	1.081	1.958	2.532	2.234	10.99	
Δ	-	3.0%	2.4%	0.4%	2.0%	
BS	1.188	1.800	2.687	2.253	11.50	0.795
BFGM	1.188	1.884	2.589	2.241	11.16	
Δ	-	4.6%	3.6%	0.5%	3.0%	
BS	1.284	1.700	2.799	2.263	11.86	0.859
BFGM	1.284	1.819	2.645	2.248	11.33	
Δ	-	12.0%	5.5%	0.7%	4.5%	
BS	1.494	1.400	3.337	2.307	14.17	1.000
BFGM	1.494	1.679	2.788	2.264	11.79	
Δ	-	20.0%	18.8%	2.0%	17.0%	
EOS L ($M_{bar} = 3.16 M_{\odot}$)						
CST	0	1.470	4.676	2.700	13.70	0
BFGM	0	1.486	4.530	2.662	13.63	
Δ	-	1.6%	3.0%	1.4%	0.5%	
CST	0.352	1.201	4.959	2.706	14.20	0.341
BFGM	0.352	1.220	4.786	2.668	14.09	
Δ	-	1.6%	3.5%	1.4%	0.8%	
CST	0.714	0.955	5.554	2.733	15.24	0.692
BFGM	0.714	0.990	5.211	2.689	14.84	
Δ	-	3.6%	6.0%	1.6%	2.6%	
CST	0.909	0.802	6.292	2.765	16.57	0.880
BFGM	0.909	0.896	5.545	2.707	15.46	
Δ	-	8.4%	11.8%	2.1%	6.7%	
CST	0.997	0.710	7.024	2.792	18.05	0.966
BFGM	0.997	0.852	5.724	2.715	15.82	
Δ	-	20.0%	18.5%	2.8%	12.4%	
CST	1.032	0.655	7.659	2.813	20.66	1.000
BFGM	1.032	0.835	5.800	2.720	15.98	
Δ	-	27.0%	24%	3.3%	23.0%	

therefore in this paper it is the sum of two contributions: $I^{(0)}$, of order Ω^0 coming from J computed at order Ω , and δI , of order Ω^2 coming from δJ computed at order Ω^3 ; in this sense we refer to I as to a quantity computed up to 3rd-order in Ω .

It should be noted that a difference of the order of a percent between quantities computed by integrating the exact or the perturbed equations can be attributed essentially to interpolation of the EOS that are given in a tabulated form. The discrepancies are indeed of that order when $\nu = 0$, with the only exception of ϵ_c of the maximum mass star for APR2. The larger discrepancy found in this case ($\Delta = 5.7\%$) can be explained noting that the APR2 model yields a $M(\epsilon_c)$ curve featuring an extended plateau around $M = M_{max}$. For example, a 7% change of the central density, from $2.65 \times 10^{15} g/cm^3$ to $2.85 \times 10^{15} g/cm^3$, only leads to a variation of the fifth digit in the value of the mass.

From Table II we see that for the stars of sequence A a critical quantity in the comparison between the exact and perturbative approach is the equatorial radius of the star; indeed, while the relative error $\Delta = (R_{exact} - R_{perturb.})/R_{exact}$ is smaller than 4.5% for $\nu \lesssim 0.85 \nu_{ms}$, it becomes of the order of 19 – 20% at mass-shedding. The reason of this discrepancy is that when the spin frequency approaches the mass-shedding limit the numerical integration of the exact equations shows that a cusp forms on the equatorial plane, from which the star starts losing matter [11]. This cusp is hardly reproduced by a perturbative expansion, and in any event it cannot be reproduced by truncating the expansion to order Ω^3 . The physical quantity which is more sensitive to the error on the radius at mass-shedding is the moment of inertia ($\sim 14\%$). From Table II it also emerges that the agreement between exact calculations and 3rd-order perturbative approach is better for the EOS APR2, which is stiffer than AU and L.

For the maximum mass sequences B, Table III shows that the discrepancies are larger; the largest error is on the central density, and the reason is the following. In order to construct a constant baryonic mass sequence, for a fixed value of ν the central density is changed until the required mass is reached; since approaching the maximum mass

$$\lim_{M \rightarrow M_{max}} \frac{\partial \epsilon_c}{\partial M_{bar}} = \infty, \quad (32)$$

when $M = M_{max}$ the determination of ϵ_c becomes less accurate.

In Table IV we show the mass-shedding frequency computed by the perturbative and the exact approach for the sequences A and B: the values we find are systematically higher than those found with the exact codes. The discrepancy has to be attributed to the inaccuracy of the perturbative approach near mass-shedding as explained above.

However, it should be stressed that the rotation rate of known pulsars is much lower than the mass-shedding

TABLE IV: The mass-shedding spin frequencies are given for sequences A and B (see text) and for the considered EOS.

ν_{ms} in KHz			
Sequence A			
	EOS AU	EOS L	EOS APR2
BFGM	1.533	0.876	1.299
CST	1.257	0.716	-
BS	1.237	0.728	1.041
Δ_{CST}	22.0%	22.3%	-
Δ_{BS}	23.9%	20.3%	24.8%
Sequence B			
	EOS AU	EOS L	EOS APR2
BFGM	2.057	1.277	1.842
CST	1.685	1.032	-
BS	1.682	1.022	1.494
Δ_{CST}	22.1%	23.7%	-
Δ_{BS}	22.3%	24.9%	23.3%

limit computed for most equation of state considered in the literature; for instance, the rotation rate of the fastest isolated pulsar observed so far is $\nu \sim 641$ Hz, and unless we are specifically interested in the mass-shedding problem, the results given in Tables II and III show that the perturbative approach can be used to study the structural properties of the observed rapidly rotating neutron stars. Indeed, for $\nu \sim 641$ Hz we find that the results of the perturbative and exact calculations for the EOS AU and APR2 differ by at most $\sim 2\%$ for all computed quantities, even for the maximum mass.

For the EOS L, differences are larger, mainly because $\nu = 641$ Hz is closer to the mass-shedding frequency than for the other EOS, and the perturbative approach becomes less accurate for the reasons explained above. In addition, unlike the EOS AU and APR2, the EOS L is tabulated with very few points, especially at high densities (only four points for $\epsilon_c > 10^{15} g/cm^3$), and this introduces further differences which depend on the interpolation scheme.

The results of Hartle’s approach have been compared to the exact results by several authors [6],[7],[9]. In all these papers the perturbative approach is developed up to order Ω^2 .

[6] focuses on the calculation of the mass-shedding frequency for the maximum mass configuration Ω_{lim} , which is computed for a number of EOS to see whether the scaling law defined in [18] and based on the results of the integration of the exact equations, is satisfied. The authors found mass-shedding frequencies systematically larger by $\sim 10 - 15\%$ than those obtained from the “exact” scaling law.

In [7], Hartle’s procedure was applied to construct models of stars rotating at mass-shedding for three values of the mass and for EOS different from those we consider. The results were compared with those of [17] where the exact equations were integrated for the same EOS, find-

ing that Hartle’s approach leads to results compatible to exact calculations down to rotational periods of the order of 0.5 ms. However, this result was subsequently disclaimed in [12], where it was shown that the equatorial radius computed by the exact codes of [17] was systematically underestimated, leading to larger values of Ω_{ms} . For this reason the agreement between [7] and [17] was good. The conclusion of [12] is that Hartle’s method to order Ω^2 cannot be considered very accurate in configurations approaching the mass-shedding limit, as we also find.

Finally, in [9] the second order Hartle’s approach is applied to construct sequences of stellar models with constant M_{bar} and varying Ω for the same five EOS used to integrate the exact codes of [14]. They used a procedure different from ours, matching the angular momentum and gravitational mass computed by the two approaches varying ν and ϵ_c . Therefore in their approach J (computed to order Ω) and M_{grav} are equal by construction. The comparison between the perturbative and the exact approaches is focused on the quadrupole moment Q , which is the coefficient of the $r^{-3}P_2(\cos\theta)$ term in Newtonian potential [3]. To order Ω^2 , Q is

$$Q = \frac{J^2}{M} + \frac{8}{5}KM^3 \quad (33)$$

where K is defined in eq. (A22). They found a relative error which depends on the EOS and increases with the rotation rate. For rates of the order of the fastest pulsar they found errors of the order of 20%. Our calculations of Q for the EOS APR2, AU and L that are also used in [14] show a much better agreement with the exact results, with a relative error smaller than 2% for $M_{grav} = 1.4 M_\odot$.

IV. THE EOS

As stated in Section I, in this work we have employed different models of the EOS of neutron star matter in the region of supranuclear density, corresponding to the star core, while the description of the outer and inner crust provided by the EOS of Refs. [15] and [16], respectively, has been kept fixed. The four EOS considered in the core have been obtained within two approaches, nuclear many body theory (NMBT) and relativistic mean field theory (RMFT), based on different dynamical assumptions and different formalisms.

The NMBT approach rests on the premise that nuclear matter can be described as a collection of nonrelativistic nucleons, interacting through phenomenological two- and three-body forces. While suffering from the obvious limitations inherent in its nonrelativistic nature, this approach is made very attractive by its feature of being strongly constrained by the data. The two-nucleon potential provides a quantitative account of the properties of the two-nucleon system, i.e. deuteron properties and ~ 4000 accurately measured nucleon-nucleon scattering

phase shifts [24], while the inclusion of the three-nucleon potential allows one to reproduce the binding energies of the three-nucleon bound states [25], as well the empirical equilibrium properties of symmetric nuclear matter [22]. Calculations of the energies of the ground and low-lying excited states of nuclei with mass number $A \leq 10$ [26], whose results are in excellent agreement with the experimental values, have also shown that NMBT has a remarkable predictive power.

Within RMFT, based on the formalism of relativistic quantum field theory, nucleons are described as Dirac fermions interacting through meson exchange. In its simplest implementation the dynamics is described by a scalar and a vector meson field [27]. This approach is very elegant, but leads to a set of equations of motion that turns out to be only tractable in the mean field approximation, i.e. treating the meson fields as classical fields. The meson masses and coupling constant are then fixed fitting the equilibrium properties of nuclear matter.

Both NMBT and RMFT can be generalized to take into account the possible appearance of strange baryons, produced in weak interaction processes that may become energetically favourable at high density. However, the inclusion of baryons other than protons and neutrons entails a large uncertainty, as little is known of their interactions and the available models are only loosely constrained by few data.

Of the four EOS we consider, those referred to as APR2 (also used in Section III to compare our results with those of non-perturbative approaches), BSS1 and BSS2 are based on NMBT, while the one labelled G240 has been obtained from RMFT. The APR2 and BSS1 EOS include nucleons only, and their differences are mainly ascribable to the approximate treatment of the three-nucleon interactions in the BSS1 model and to the presence of relativistic boost corrections in the APR2 model. The BSS2 model is a generalization of BSS1 including the hyperons Σ^- and Λ^0 . Finally, the G240 EOS includes the full baryon octet, consisting of protons, neutrons and $\Sigma^{0,\pm}$, Λ^0 and Ξ^\pm .

The non rotating neutron star configurations corresponding to the APR2 and BSS1 EOS exhibit similar mass-radius relations, with a maximum gravitational mass $\gtrsim 2 M_\odot$. The appearance of strange baryons makes the EOS softer, thus leading to sizable changes in the mass-radius relation. This feature is clearly visible in the case of both the BSS2 and G240 EOS [28], and leads to maximum masses of $\sim 1.22 M_\odot$ and $\sim 1.55 M_\odot$, respectively.

Comparison with the experimental determinations of the masses of neutron stars located in binary radio pulsar systems, yielding a narrow distribution centered at $1.35 \pm 0.04 M_\odot$ [29], suggests that the dynamics underlying the BSS2 model leads to too soft an EOS. On the other hand, all other EOS appear to be compatible with the mass of the most massive neutron star listed in Ref. [29] ($\sim 1.56 M_\odot$).

V. RESULTS

Using the above EOS to describe matter in the crust and in the stellar core, and using the procedure developed in section II, the equations of stellar structure perturbed to order Ω^3 have been integrated to construct sequences of stellar configurations with constant baryonic mass and varying angular velocity. In our study we consider six values of M_{bar} , plus the maximum mass model for each EOS. The gravitational mass is

$$M_{grav} = M + \delta M_{grav} + O(\Omega^4), \quad (34)$$

where

$$M = 4\pi \int_0^R r^2 \epsilon(r) dr \quad (35)$$

is the gravitational mass of the non rotating configuration and δM_{grav} is given by eq. (14); M_{grav} depends on the EOS and on the angular velocity. In Table V for each EOS we give the values of M for the non rotating model that corresponds to the selected M_{bar}

TABLE V: For each value of the baryonic mass in column 1, the corresponding values of the gravitational mass of the non rotating configuration are tabulated for the selected EOS.

M_{bar}/M_\odot	M/M_\odot			
	APR2	BBS1	BBS2	G240
1.31	1.19	1.18	1.19	1.20
1.50	1.35	1.34	-	1.37
1.56	1.39	1.38	-	1.41
1.68	1.49	1.47	-	1.51
2.10	1.80	1.79	-	-
2.35	2.00	1.97	-	-

TABLE VI: Maximum masses of the non rotating configurations.

EOS	M_{bar}^{max}/M_\odot	M^{max}/M_\odot
APR2	2.70	2.20
BBS1	2.41	2.01
BBS2	1.74	1.22
G240	1.35	1.55

The maximum masses (baryonic and gravitational) of the non rotating configurations are given in Table VI for the selected EOS.

An example of how the gravitational mass changes due to rotation is shown in Fig. 1, where we plot M_{grav} (in solar mass units) as a function of the central density for different values of the spin frequency for the EOS APR2, evidentiating the sequencies with $M_{bar} = const.$

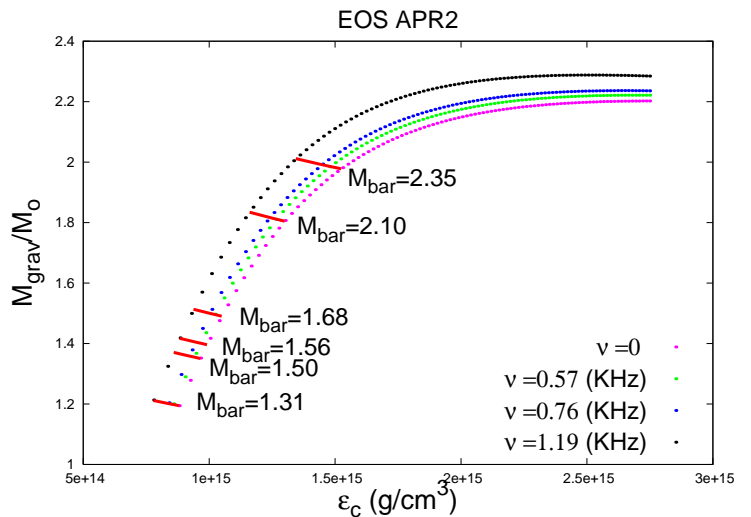


FIG. 1: (Color online) The gravitational mass for the EOS APR2 is plotted as a function of the central density for different values of the spin frequency, evidentiating the curves with $M_{bar} = const.$

A. Mass-shedding limit

In Fig. 2 we plot the mass-shedding frequency, ν_{ms} , as a function of the gravitational mass for each EOS. The dashed horizontal line is the frequency of PSR 1937+21, the fastest isolated pulsar observed so far, the mass of which is presently unknown.

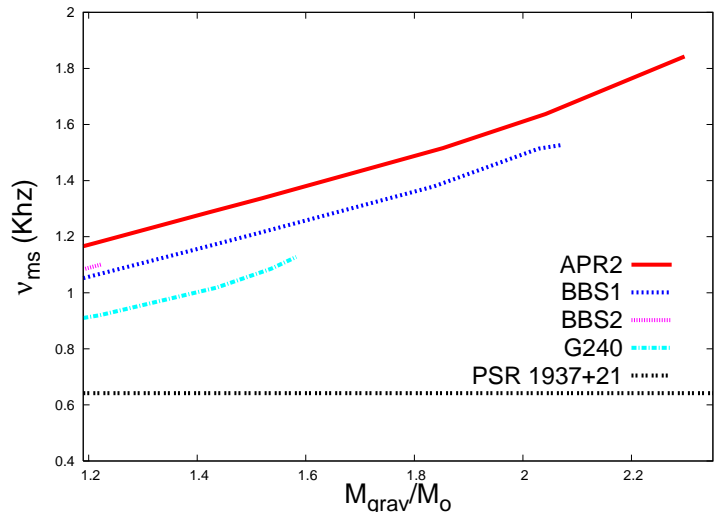


FIG. 2: (Color online) The mass-shedding frequency ν_{ms} is plotted for each EOS as a function of the gravitational mass. The horizontal line corresponds to the spin frequency of PSR 1937+21, which is the fastest isolated pulsar observed so far and whose mass is presently unknown.

We see that the values of ν_{ms} for G240 are systematically lower than those of the other EOS, while those

for APR2 are systematically higher. This behaviour can be understood from the data given in Table VII where, for each EOS, we tabulate the ratio of the gravitational mass of the star rotating at mass-shedding to the equatorial radius, $M_{grav}^{ms}/R_{eq}^{ms}$, for three values of the baryonic mass. For a given mass, the ordering of ν_{ms} in Fig. 2 corresponds to the same ordering of $M_{grav}^{ms}/R_{eq}^{ms}$ in Table VII, showing that more compact stars admit a higher mass-shedding limit.

TABLE VII: For each EOS and for three values of the baryonic mass, we tabulate the ratio of the gravitational mass of the star rotating at mass-shedding to the equatorial radius, $M_{grav}^{ms}/R_{eq}^{ms}$. In the last three columns, we give the ratio M/R for the non rotating star with the same baryonic mass.

	$\nu = \nu_{ms}$			$\nu = 0$		
	$M_{grav}^{ms}/R_{eq}^{ms}$			M/R		
M_{bar}/M_{\odot}	1.31	1.56	2.35	1.31	1.56	2.35
G240	0.106	0.127	-	0.131	0.163	-
BBS1	0.114	0.136	0.210	0.143	0.169	0.267
BBS2	0.117	-	-	0.154	-	-
APR2	0.124	0.147	0.223	0.152	0.179	0.268

In the last three column of Table VII we also give the ratio M/R of the non rotating star with the same baryonic mass, and it is interesting to see that rotation affects the compactness of a star in a way which depends on the EOS. For instance, for $M_{bar} = 1.31M_{\odot}$ (for which all EOS admit a stable configuration), the non rotating star with EOS BBS2 ($M/R = 0.154$) is more compact than that with EOS APR2 ($M/R = 0.152$), while near mass-shedding the compactness of the BBS2 star ($M_{grav}^{ms}/R_{eq}^{ms} = 0.117$) is smaller than that of the APR2 star ($M_{grav}^{ms}/R_{eq}^{ms} = 0.124$).

To further clarify this behaviour in Fig. 3 we plot the energy density inside the star as a function of the radial distance for these two EOS in the non rotating case and at mass-shedding. It is useful to remind that the main difference between the EOS APR2 and BBS2 is that in the core of the BBS2 star there are hyperons. From the upper panel of Fig. 3 we see that when the BBS2 star does not rotate hyperons are highly concentrated in the core, making the central density very large; however, since the EOS is soft, when the star rotates fastly matter is allowed to distribute throughout the star. Conversely, due to the stiffness of the APR2 EOS, in the corresponding star (Fig. 3 lower panel) the matter distribution does not seem to be so affected by rotation. A similar analysis can be found in [17] were different EOS were considered.

By comparing our results to order Ω^3 with those to order Ω^2 we find that the third order contributions to the mass-shedding limit are actually negligible, smaller than 1%, independently of the EOS.

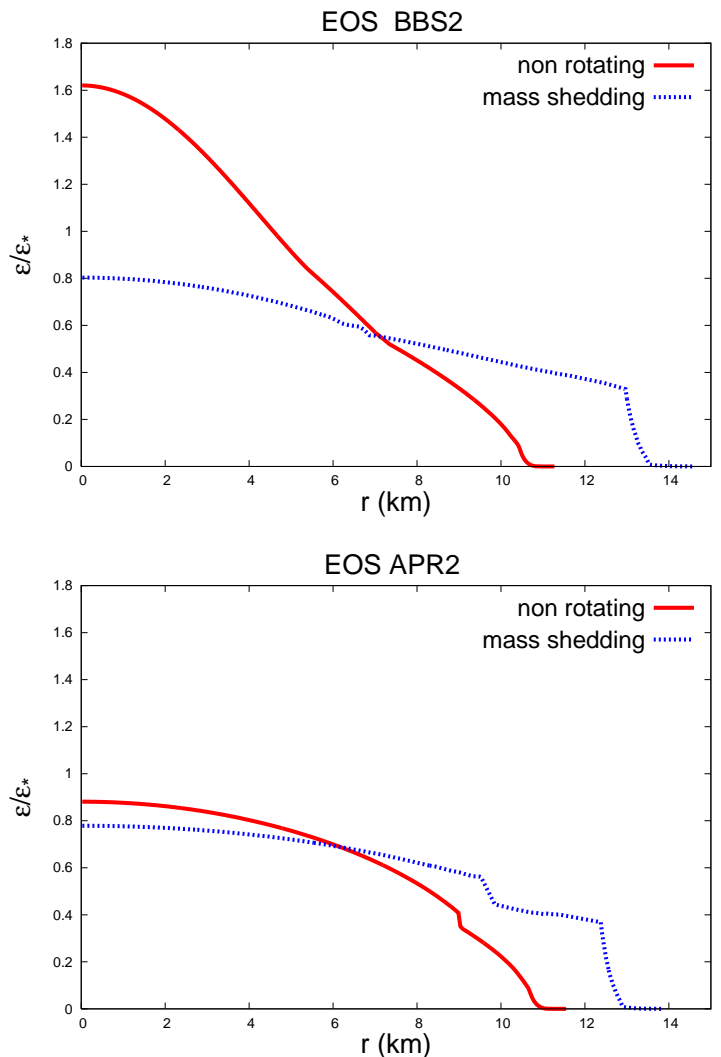


FIG. 3: (Color online) The energy density distribution inside the star is plotted as a function of the radial distance for the EOS APR2 and BBS2, and for $M_{bar} = 1.31$. ϵ is given in units of $\epsilon_* = 10^{15} g/cm^3$. In both cases the continuous line refers to the non rotating configuration, the dotted line to the star rotating at mass-shedding.

B. Estimates of the moment of inertia

In Fig. 4 we plot the moment of inertia as a function of the spin frequency, for each EOS and for given values of the baryonic mass up to the maximum mass. Since we know, as discussed in section III, that the mass-shedding frequencies estimated by our perturbative approach are about 20% larger than those found by integrating the exact equations, we plot the data only for $\nu < 80\% \nu_{ms}$, where ν_{ms} is the mass-shedding frequency we find. From Fig. 4 we see that the moment of inertia has a non-trivial behaviour as the baryonic mass increases. Indeed, along a $\Omega = constant$ sequence of stellar models, if $M_{bar} \ll M_{bar}^{max}$ then I is an *increasing* function of M_{bar} ,

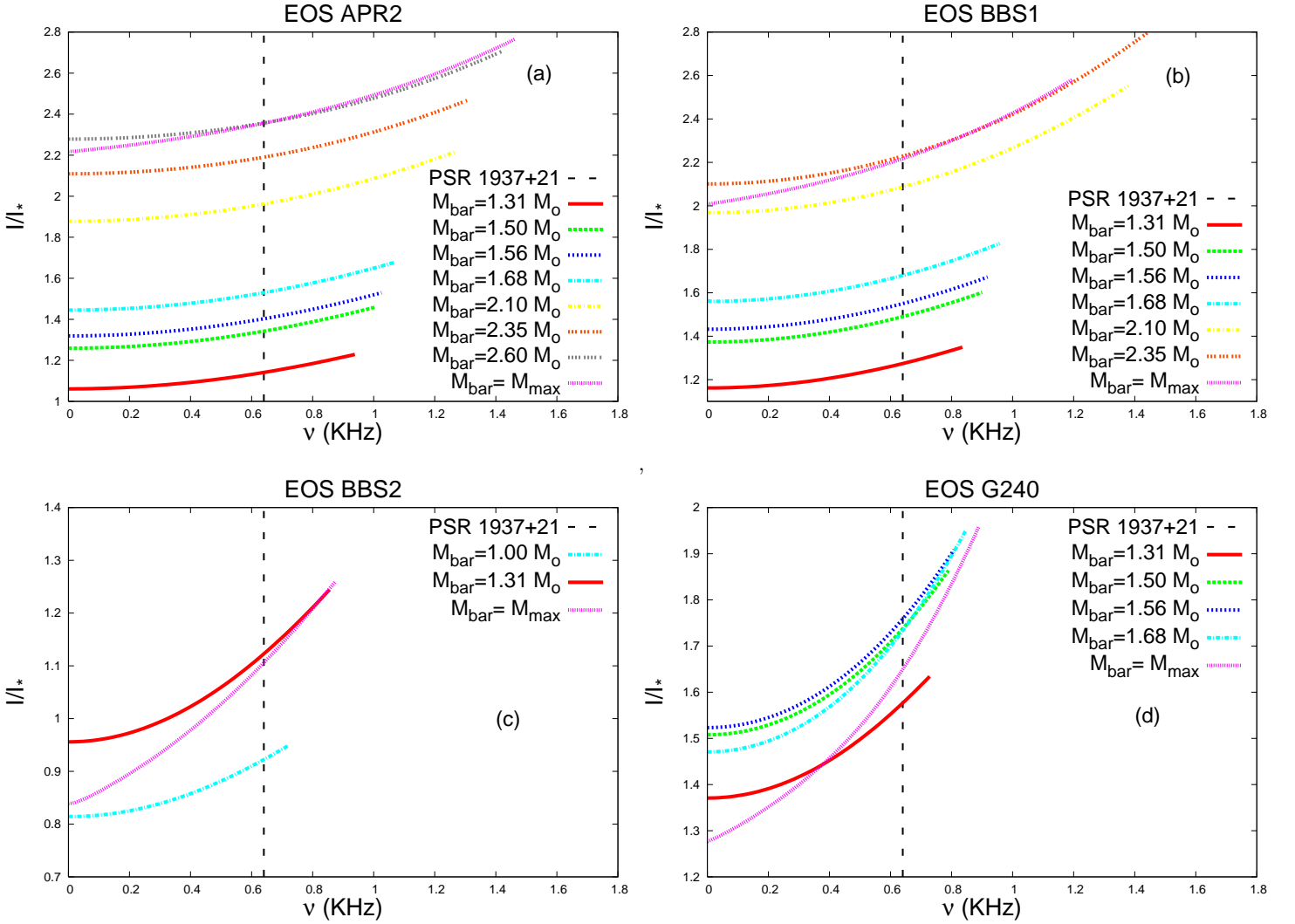


FIG. 4: (Color online) The moment of inertia (in units of $I_* = 10^{45} \text{ g cm}^2$) is plotted as a function of the spin frequency, for the EOS APR2 (panel a), BBS1 (panel b), BBS2 (panel c) and G240 (panel d). For each EOS we consider a few values of the baryonic mass up to the maximum mass, and plot the data only for $\nu \leq 80\% \nu_{ms}$ (see text). The vertical dashed line is the spin frequency of PSR 1937+21.

while as M_{bar} approaches the maximum mass I becomes a *decreasing* function of M_{bar} .

This behaviour can be understood as follows: $I \sim MR^2$, and while in general keeping Ω constant as the mass increases the radius decreases, approaching the maximum mass the mass remains nearly constant while the radius is continuously decreasing. This is true for any EOS, but of course it is more evident for softer EOS like BBS2 and G240.

In a recent paper [30] it has been suggested that a measurement of the moment of inertia from pulsar timing data will impose significant constraints on the nuclear EOS. The authors consider the newly discovered binary double pulsar PSR J037-3039, and construct models of the fastest pulsar ($M = 1.337 M_\odot$, $\nu = 276.8 \text{ Hz}$) with different EOS. They compute the moment of inertia as-

suming the star is rigidly rotating using the fully non linear, numerical code developed in [13], and compare the results with those obtained using Hartle’s perturbative approach developed at first order in the angular velocity, i.e. they compute the quantity given in eq. (31) which we call $I^{(0)}$. They show that the agreement is very good, and this had to be expected since the spin frequency of the considered star is quite low. What we want to show now is that if we consider stars that rotate faster, as for example PSR 1937+21, the first order approach is inaccurate, and we need to consider the third order corrections. To this purpose, in Fig. 5 we plot for each EOS and for $M_{bar} = 1.56 M_\odot$ the first order term $I^{(0)}$ (dashed line) and $I = I^{(0)} + \delta I$ (solid line) where δI is the correction found by solving the perturbed equations to order Ω^3 . For each EOS, the data are plotted for $\nu \leq 80\% \nu_{ms}$.

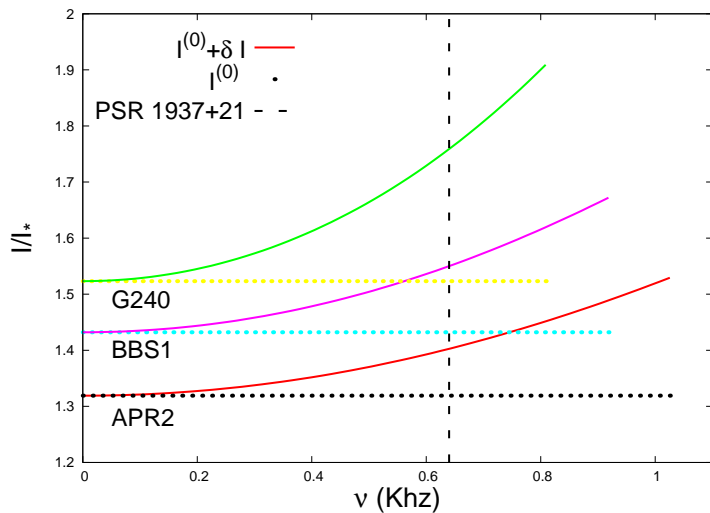


FIG. 5: (Color online) The moment of inertia, measured in units of $I_* = 10^{45} \text{ g cm}^2$, is plotted versus the spin frequency (in KHz) for stars with baryonic mass $M_{bar} = 1.56 M_\odot$. The continuous lines refer to I computed by solving the stellar structure equations to third order in the angular velocity, whereas the horizontal dashed lines refer to the first order term $I^{(0)}$. The vertical dashed line is the spin frequency of PSR 1937+21. For each EOS, the data are plotted only for $\nu \leq 80\% \nu_{ms}$ (see text).

The vertical dashed line refers to the spin frequency of PSR 1937+21. It is clear from the figure that the third order correction becomes relevant at frequencies higher than $\sim 0.5 \text{ KHz}$. For instance if $\nu = 641 \text{ Hz}$ the relative error $[\delta I / (I^{(0)} + \delta I)]$ that one makes neglecting the third order corrections are 5% for APR2, 7% for BBS1 and 13% for G240.

It is interesting to compare $I^{(0)}$, $I = I^{(0)} + \delta I$, where δI is computed using corrections of order Ω^3 , and the value of I one gets by integrating the exact equations of stellar structure. This is possible for the EOS APR2 and the results are shown in Table VIII for $M_{grav} \sim 1.4 M_\odot$ and $\nu = 644 \text{ Hz}$, and for the maximum mass and $\nu = 609 \text{ Hz}$.

The table shows that including third order is important to adequately estimate the moment of inertia of the fastest pulsars.

VI. CONCLUDING REMARKS

In this paper we have solved the equations of stellar structure developed to third order in the angular velocity, using recent EOS which model hadronic interactions in different ways to describe the matter in the inner core. The stellar parameters we find have been compared, when available in the literature, with those found by solving the exact equations of stellar structure. The main conclusions we can draw from our study are the following.

It is known that near mass-shedding the perturbative

TABLE VIII: We compare the moment of inertia computed for the EOS APR2 by integrating the exact equations of stellar structure (column 2) [14], the perturbed equations to order Ω (column 3), and to order Ω^3 (column 5). The relative error between the exact and the approximated results are given in columns 4 and 6. I is in units of $I_* = 10^{45} \text{ g cm}^2$.

	I_{exact}/I_*	$I^{(0)}/I_*$	Δ	$(I^{(0)} + \delta I)/I_*$	Δ
$M_{grav} \sim 1.4 M_\odot$ $\nu = 644 \text{ Hz}$	1.425	1.238	13%	1.395	2.1%
	I_{exact}/I_*	$I^{(0)}/I_*$	Δ	$(I^{(0)} + \delta I)/I_*$	Δ
$M_{grav} = M_{max}$ $\nu = 609 \text{ Hz}$	2.352	2.281	3%	2.347	0.2%

approach fails to correctly reproduce the stellar properties and the reasons are well understood. We confirm this behaviour and give quantitative results in this limit.

However, for lower values of the angular velocity the situation is different. Taking as a reference the rotation rate of the fastest isolated pulsar observed so far, PSR 1937+21, for which $\nu \sim 641 \text{ Hz}$, we see that at these rates the perturbative approach allows to describe all stellar properties to an accuracy better than $\sim 2\%$ even for the maximum mass models, unless the EOS in the core is very soft, as in the case of the EOS L; indeed, for this EOS the mass-shedding velocity is low and close to the chosen rotation rate, so that the perturbative approach is inaccurate.

The two quantities that are affected by third order corrections are the mass-shedding velocity and the moment of inertia. For the first, we find that the third order corrections are actually negligible, smaller than 1%, independently of the EOS.

Conversely, the moment of inertia is affected by terms of order Ω^3 in a significant way; for instance, for a star with $M = 1.4 M_\odot$ rotating at $\nu \sim 641 \text{ Hz}$ the third order correction is of the order of $\delta I / (I^{(0)} + \delta I) \sim 5\%$ for the stiffer EOS we use (APR2), and as high as $\sim 13\%$ for the softest (G240).

Thus, third order corrections have to be included to study the moment of inertia of rapidly rotating neutron stars, whereas they are irrelevant to estimate the mass-shedding limit.

APPENDIX A

In this appendix we write the equations that govern the radial part of the metric and thermodynamical functions that describe the structure of a rotating star to third order in the angular velocity Ω . For each function we specify the appropriate boundary conditions and we show how to construct the solution order by order. We give explicitly the analytic solution when available, following and completing the work of Hartle and collaborators [1,

2, 3]. In what follows we shall refer to the functions appearing in section II.

We recall that the structure of a non rotating, spherical star is described by the TOV equations

$$\begin{aligned}\frac{dM(r)}{dr} &= 4\pi r^2 \epsilon(r), \\ \frac{d\nu(r)}{dr} &= 2 \frac{M(r) + 4\pi r^3 P(r)}{r(r - 2M(r))}, \\ \frac{dP(r)}{dr} &= - \frac{(P(r) + \epsilon(r))}{2} \nu(r),_{,r}.\end{aligned}\quad (\text{A1})$$

$\epsilon(r)$ and $P(r)$ are the energy density and pressure distribution in the non rotating star. Since all functions we shall consider depend on r , we shall omit this dependency throughout.

Hereafter, R and $M(R)$ will indicate, respectively, the radius and the mass of the non rotating star, found by solving eqs. (A1) for an assigned EOS.

1. The first order equations

To order Ω the shape of the star remains spherical and there is only one function, ω , to determine, which is responsible for the dragging of inertial frames (cfr. the expansion in eq. 6). By introducing the function $\varpi = \Omega - \omega$, it is easy to show that it satisfies the following equation [1]

$$\frac{1}{r^4} \frac{d}{dr} (r^4 j \frac{d\varpi}{dr}) + \frac{4}{r} \frac{dj}{dr} \varpi = 0, \quad (\text{A2})$$

where $j(r) = e^{-\nu/2} \sqrt{1 - \frac{2M}{r}}$. Equation (A2) can be reduced to two first order equations by defining two auxiliary functions of r

$$\chi = j\varpi, \quad u = r^4 j \frac{d\varpi}{dr} \quad (\text{A3})$$

that satisfy

$$\begin{aligned}r \leq R \quad \frac{d\chi}{dr} &= \frac{u}{r^4} - \frac{4\pi r^2 (\epsilon + P)\chi}{r - 2M} \\ \frac{du}{dr} &= \frac{16\pi r^5 (\epsilon + P)\chi}{r - 2M}.\end{aligned}\quad (\text{A4})$$

They have to be integrated from $r = 0$ to R with the following boundary conditions

$$\chi(0) = j(0)\varpi_c, \quad u(0) = 0. \quad (\text{A5})$$

These conditions follow from the behaviour of ϖ near the origin

$$\varpi \sim \varpi_c (1 + \varpi_2 r^2 + \dots), \quad (\text{A6})$$

where ϖ_c is a constant. Note that from eqs. (A3) and (A6) it follows that u goes to zero faster than r^4 .

For $r \geq R$, P and ϵ vanish, $M \equiv M(R)$, and the solution of eqs. (A4) is

$$r \geq R \quad \chi(r) = \Omega - \frac{2J}{r^3}, \quad u(r) = 6J, \quad (\text{A7})$$

where J is a constant which represents the angular momentum of the star to first order in Ω . The constants ϖ_c and J can be found by imposing that the interior and the exterior solutions match continuously at R , i.e.

$$\varpi_c \chi(R) = \Omega - \frac{2J}{R^3}, \quad u(R) = 6J.$$

2. Second order equations

The second order terms affect the structure of the star in the following way: h_0 and m_0 produce a spherical expansion, h_2 and v_2 a quadrupole deformation.

On the assumption that the EOS is a one parameter equation of state, Einstein's equations admit a first integral (cfr. [1]) that allows to find two equations, one relating h_0 and δp_0 , the second h_2 and δp_2 . These two equations are

$$\bar{\mu} = \delta p_0 + h_0 - \frac{1}{3} e^{-\nu} r^2 \varpi^2 \quad (\text{A8})$$

$$0 = \delta p_2 + h_2 + \frac{1}{3} e^{-\nu} r^2 \varpi^2, \quad (\text{A9})$$

where $\bar{\mu}$ is the correction of order Ω^2 to the chemical potential μ_c

$$\mu_c = \mu [1 + \bar{\mu} + O(\Omega^4)] \equiv \frac{\mathcal{E} + \mathcal{P}}{u^t} \exp \left[- \int \frac{d\mathcal{E}}{\mathcal{E} + \mathcal{P}} \right] \quad (\text{A10})$$

(where \mathcal{E} and \mathcal{P} are the energy density and pressure in the rotating configuration) which can be shown to be constant with respect to r and θ throughout the star.

a. Spherical expansion

Using eq. (A8), the relevant equations for the spherical deformation can be shown to be

$$\begin{aligned}\frac{dm_0}{dr} &= 4\pi r^2 \frac{d\epsilon}{dP} [\delta p_0 (\epsilon + P)] + \frac{u^2}{12r^4} + \frac{8\pi r^5 (\epsilon + P)\chi^2}{3(r - 2M)} \\ \frac{d\delta p_0}{dr} &= \frac{u^2}{12r^4 (r - 2M)} \\ &- \frac{m_0 (1 + 8\pi r^2 P)}{(r - 2M)^2} - \frac{4\pi (\epsilon + P) r^2 \delta p_0}{r - 2M} \\ &+ \frac{2r^2 \chi}{3(r - 2M)} \left[\frac{u}{r^3} + \frac{(r - 3M - 4\pi r^3 P)\chi}{r - 2M} \right]\end{aligned}\quad (\text{A11})$$

where u and χ are defined in (A3). These equations must be integrated inside the star from $r = 0$ to R with the condition that both m_0 and δp_0 vanish in $r = 0$. To start

the numerical integration it is useful to make use of the following expansion

$$\begin{aligned} m_0(r) &\sim \frac{4\pi}{15} [\epsilon(0) + P(0)] \left[\left(\frac{d\epsilon}{dP} \right)_{r=0} + 2 \right] \chi(0)^2 r^5 \\ \delta p_0(r) &\sim \frac{1}{3} \chi(0) r^2, \quad r \rightarrow 0. \end{aligned} \quad (\text{A12})$$

For $r \geq R$ u and χ reduce to (A7); by integrating the first eq. (A11) with P and ϵ vanishing, one finds

$$m_0(r) = -\frac{J^2}{r^3} + \delta M \quad (\text{A13})$$

where δM is a constant which represents the correction to the gravitational mass due to the spherical expansion of the star. This quantity can be determined by imposing the continuity of the solution at $r = R$, i.e.

$$\delta M = m_0(R) + \frac{J^2}{R^3}, \quad (\text{A14})$$

and $m_0(R)$ is found by integrating eqs. (A11) for $r \leq R$.

Due to the spherical expansion, the pressure of each element of fluid changes by an amount $\delta p_0(r)$ found by integrating eqs. (A11); at the same time the element is radially displaced by an amount

$$r + \xi_0(r), \quad (\text{A15})$$

and $\xi_0(r)$ can be found in terms of $\delta p_0(r)$ using eq. (9); known $\xi_0(r)$ we can compute the corresponding variation of the stellar radius (cfr. eq. 12)

$$\delta R^A = \xi_0(R) = \frac{\delta p_0(R) R (R - 2M(R))}{M(R)}. \quad (\text{A16})$$

b. Quadrupole deformation

We shall now solve the equations for $h_2(r)$ e $v_2(r)$, that are responsible for the quadrupole deformation of the star:

$$\begin{aligned} \frac{dv_2}{dr} &= -\frac{d\nu}{dr} h_2 + \left(\frac{1}{r} + \frac{1}{2} \frac{d\nu}{dr} \right) \left[\frac{8\pi r^5 (\epsilon + P) \chi^2}{3(r - 2M)} + \frac{u^2}{6r^4} \right] \\ \frac{dh_2}{dr} &= \left[-\frac{d\nu}{dr} + \frac{r}{r - 2M} \left(\frac{d\nu}{dr} \right)^{-1} (8\pi(\epsilon + P) - \frac{4M}{r^3}) \right] h_2 \\ &\quad - \frac{4v_2}{r(r - 2M)} \left(\frac{d\nu}{dr} \right)^{-1} + \frac{u^2}{6r^5} \left[\frac{1}{2} \frac{d\nu}{dr} r - \frac{1}{r - 2M} \left(\frac{d\nu}{dr} \right)^{-1} \right] \\ &\quad + \frac{8\pi r^5 (\epsilon + P) \chi^2}{3(r - 2M)} \left[\frac{1}{2} \frac{d\nu}{dr} r + \frac{1}{r - 2M} \left(\frac{d\nu}{dr} \right)^{-1} \right]. \end{aligned} \quad (\text{A17})$$

Let us consider the solution for $r \leq R$ first.

It is easy to check that a regular solution of eqs. (A17) near the origin must behave as

$$r \rightarrow 0 \quad h_2(r) \sim Ar^2, \quad v_2 \sim Br^4, \quad (\text{A18})$$

where the constants A and B are related by the following expression

$$B + 2\pi \left[\frac{1}{3} \epsilon(0) + P(0) \right] A = \frac{2}{3} \pi [\epsilon(0) + P(0)] (j(0) \varpi_c)^2. \quad (\text{A19})$$

Following [1], we write the general solution of eqs. (A17) for $r \leq R$ as

$$\begin{aligned} h_2(r) &= h_2^P + C h_2^H \\ v_2(r) &= v_2^P + C v_2^H. \end{aligned} \quad (\text{A20})$$

C is a constant to be determined (see below), (h_2^P, v_2^P) are a particular solution found by integrating eqs. (A17) with the initial conditions, say, $A = 1$ and B given by eq. (A19); (h_2^H, v_2^H) are the solution of the homogeneous system which is found by putting $\chi = 0$ and $u = 0$ in eqs. (A17), numerically integrated with the boundary condition

$$r \rightarrow 0 \quad h_2^H(r) \sim r^2 \quad (\text{A21})$$

$$v_2^H(r) \sim -2\pi \left[\frac{1}{3} \epsilon(0) + P(0) \right] r^4.$$

For $r \geq R$ eqs. (A17) can be solved analytically in terms of the associated Legendre functions of the second kind, and the solution is [1],[3]

$$\begin{aligned} r \geq R \quad h_2(r) &= J^2 \left(\frac{1}{M(R)r^3} + \frac{1}{r^4} \right) + K Q_2^2(\xi) \\ v_2(r) &= -\frac{J^2}{r^4} + K \frac{2M(R)}{[r(r - 2M(R))]^{1/2}} Q_2^1(\xi) \end{aligned} \quad (\text{A22})$$

where K is a constant and

$$\begin{aligned} Q_2^2(\xi) &= \left[\frac{3}{2} (\xi^2 - 1) \log \left(\frac{\xi + 1}{\xi - 1} \right) - \frac{3\xi^3 - 5\xi}{\xi^2 - 1} \right] \\ Q_2^1(\xi) &= (\xi^2 - 1)^{1/2} \left[\frac{3\xi^2 - 2}{\xi^2 - 1} - \frac{3}{2} \xi \log \left(\frac{\xi + 1}{\xi - 1} \right) \right]. \end{aligned} \quad (\text{A23})$$

with

$$\xi = \frac{r}{M(R)} - 1. \quad (\text{A24})$$

We can now determine the constants C and K by imposing that the solution (A20) and the solution (A22) are equal at $r = R$; thus, the functions h_2 and v_2 are completely determined.

We can now compute the quadrupole deformation of the star. Indeed, known h_2 from eq. (A9) we find δp_2 :

$$\delta p_2(r) = -h_2(r) - \frac{1}{3} e^{-\nu(r)} r^2 \varpi(r)^2, \quad (\text{A25})$$

and from eq. (10) we find the second correction to the displacement

$$\xi_2(r) = -\delta p_2(r) / \left[\frac{1}{\epsilon + P} \frac{dP}{dr} \right]. \quad (\text{A26})$$

Thus, an element of fluid located at a given r and a given θ in the non rotating star, when the star rotates moves to a new position identified by the same value of θ , and by a radial coordinate

$$\bar{r} = r + \xi_0(r) + \xi_2(r)P_2(\theta) + O(\Omega^4), \quad (\text{A27})$$

where $\xi_0(r)$ and $\xi_2(r)$ are found as explained above.

The remaining metric function m_2 can be determined by a suitable combination of Einstein's equations, which gives

$$m_2 = (r - 2M) \left[-h_2 + \frac{8\pi r^5(\epsilon + P)\chi^2}{3(r - 2M)} + \frac{u^2}{6r^4} \right]. \quad (\text{A28})$$

3. Third order equations

The functions that describe the third order corrections are w_1 and w_3 , and satisfy two second order differential equations with a similar structure. Since they do not couple, we shall solve them independently.

a. The equations for w_1

$$\frac{1}{r^4} \frac{d}{dr} (r^4 j \frac{dw_1(r)}{dr}) + \frac{4}{r} \frac{dj}{dr} w_1 = D_0 - \frac{1}{5} D_2, \quad (\text{A29})$$

where

$$\begin{aligned} r^4 D_0 &= -u \frac{d}{dr} \left[\frac{m_0}{r - 2M} + h_0 \right] + 4r^3 \chi \left[\frac{1}{j} \frac{dj}{dr} \right] \\ &\cdot \left[\frac{2m_0}{r - 2M} + \left(\frac{1}{(dP/d\epsilon)} + 1 \right) \delta p_0 + \frac{2r^3 \chi^2}{3(r - 2M)} \right], \\ \frac{r^4 D_2}{5} &= \frac{u}{5} \frac{d}{dr} \left[4k_2 - h_2 - \frac{m_2}{r - 2M} \right] + \left(\frac{4r^3 \chi}{5} \right) \left[\frac{1}{j} \frac{dj}{dr} \right] \\ &\cdot \left[\frac{2m_2}{r - 2M} + \left(\frac{1}{(dP/d\epsilon)} + 1 \right) \delta p_2 - \frac{2r^3 \chi^2}{3(r - 2M)} \right]. \end{aligned} \quad (\text{A30})$$

By introducing the variables

$$\chi_1 = j w_1 \quad u_1 = r^4 j \frac{dw_1}{dr} \quad (\text{A31})$$

eq. (A29) becomes

$$\begin{aligned} \frac{d\chi_1}{dr} &= \frac{u_1}{r^4} - \frac{4\pi r^2(\epsilon + P)\chi_1}{r - 2M}, \\ \frac{du_1}{dr} &= \frac{16\pi r^5(\epsilon + P)\chi_1}{r - 2M} + r^4 D_0 - \frac{r^4}{5} D_2. \end{aligned} \quad (\text{A32})$$

We write the general solution of this system for $r \leq R$ as

$$\begin{aligned} \chi_1 &= \chi_1^P + C \chi_1^H \\ u_1 &= u_1^P + C u_1^H. \end{aligned} \quad (\text{A33})$$

C is a constant, (χ_1^P, u_1^P) , are a particular solution found by integrating eqs. (A32) with the initial conditions

$$\chi_1^P(0) = 0, \quad u_1^P(0) = 0;$$

(χ_1^H, u_1^H) is the solution of eqs. (A32) in which D_0 and D_2 are set to zero, numerically integrated with the asymptotic conditions

$$\begin{aligned} r \rightarrow 0 \quad \chi_1^H(r) &\sim 1 + \frac{8\pi}{5} [\epsilon(0) + P(0)] r^2, \\ u_1^H(r) &\sim \frac{16\pi}{5} [\epsilon(0) + P(0)] r^5. \end{aligned} \quad (\text{A34})$$

For $r \geq R$ eqs. (A32) reduce to

$$\begin{aligned} \frac{d\chi_1}{dr} &= \frac{u_1}{r^4}, \\ \frac{du_1}{dr} &= -\frac{u}{5} \frac{d}{dr} \left[4k_2 - \frac{6J^2}{r^4} \right]. \end{aligned} \quad (\text{A35})$$

Note that, since $j(r \geq R) = 1$, for $r \geq R$ χ_1 and w_1 coincide (cfr. eq. A31).

At large distance from the source w_1 must behave as

$$w_1(r) = \frac{2\delta J}{r^3} + O\left(\frac{1}{r^4}\right), \quad (\text{A36})$$

where δJ is the correction to the angular momentum of the star; this suggests to write w_1 , and therefore χ_1 , as

$$w_1(r) = \chi_1(r) = \frac{2\delta J}{r^3} + F(r), \quad (\text{A37})$$

where $F(r)$ must go to zero at infinity faster than r^3 . Consequently, when $r \rightarrow \infty$ $u_1 \rightarrow -6\delta J$. Thus, by direct integration of the second eq. (A35), and using eqs. (A7), (5) and (A22), we find

$$\begin{aligned} u_1^{ext} &= -\frac{u}{5} \left[4k_2 - \frac{6J^2}{r^4} \right] - 6\delta J = \frac{84J^3}{5r^4} + \frac{24J^3}{5M(R)r^3} \\ &+ \frac{24JKQ_2^2}{5} - \frac{48M(R)JKQ_2^1}{5[r(r - 2M(R))]^{1/2}} - 6\delta J. \end{aligned} \quad (\text{A38})$$

Knowing u_1^{ext} , we can now integrate the first of eqs. (A35) which, using eq. (A37), becomes an equation for $F(r)$, the solution of which is

$$\begin{aligned} F(r) &= -\frac{12J^3}{5r^7} - \frac{4J^3}{5Mr^6} + \\ &\frac{JK}{40M^3r^4} \left[108r^4 \ln\left(\frac{r}{r - 2M}\right) - 288r^3 M \ln\left(\frac{r}{r - 2M}\right) \right. \\ &+ 33r^4 - 240r^3 M + 336r^2 M^2 + 256M^3 r - 96M^4 \\ &\left. + 192rM^3 \ln\left(\frac{r}{r - 2M}\right) + 12r^4 \ln\left(\frac{r}{r - 2M}\right) \right] - \frac{33JK}{40M^3}, \end{aligned} \quad (\text{A39})$$

where $M \equiv M(R)$. This expression satisfies eq. (A35), as it can be checked by direct substitution; it may be noted that it differs from the expression of $F(r)$ given in ref. [1] which, conversely, does not satisfy eq.(A35).

In conclusion

$$\chi_1^{ext} = \frac{2\delta J}{r^3} + F(r). \quad (\text{A40})$$

At this point the situation is the following. We have integrated eqs. (A32) for $r \leq R$, and we know the solution for u_1 and χ_1 up to the constant C (eq. A33); we have found the solution for $r \geq R$ for u_1 (eq.A38) and for χ_1 (eq. A40) up to the constant δJ . The two constants are found by imposing that the solutions for u_1 and χ_1 given by eqs. (A33) and by eqs. (A38,A40) match continuously at $r = R$.

It should be noted that computing δJ by this procedure or by eq. (28) is equivalent; indeed we find a relative difference smaller than 10^{-10} . This is a further check of the correctness of the analytic expression (A39) for $F(r)$ we derived.

b. The equations for w_3

The solution for the remaining function w_3 can be found along the same path. We start with the equation

$$\frac{1}{r^4} \frac{d}{dr} (r^4 j \frac{dw_3(r)}{dr}) + \frac{4}{r} \frac{dj}{dr} w_3 - \frac{10jw_3}{r(r-2M)} = \frac{1}{5} D_2 \quad (\text{A41})$$

and assume $r \leq R$; we introduce the functions

$$\chi_3 = jw_3 \quad u_3 = r^4 j \frac{dw_3}{dr} \quad (\text{A42})$$

and find

$$\begin{aligned} \frac{d\chi_3}{dr} &= \frac{u_3}{r^4} - \frac{4\pi r^2(\epsilon + P)\chi_3}{r-2M}, \\ \frac{du_3}{dr} &= \frac{16\pi r^5(\epsilon + P)\chi_3}{r-2M} + \frac{10\chi_3 r^3}{(r-2M)} + \frac{r^4}{5} D_2. \end{aligned} \quad (\text{A43})$$

The general solution of eqs. (A43) for $r \leq R$ is

$$\begin{aligned} \chi_3 &= \chi_3^P + C \chi_3^H \\ u_3 &= u_3^P + C u_3^H. \end{aligned} \quad (\text{A44})$$

C is a constant and (χ_3^P, u_3) are a particular solution found by integrating eqs. (A43) with the initial conditions

$$\chi_3^P(0) = 0, \quad u_3^P(0) = 0,$$

(χ_3^H, u_3^H) are the solution of the homogeneous system obtained by putting $D_2 = 0$ in (A43) and integrating up to R with the boundary condition

$$r \rightarrow 0 \quad \chi_3^H(r) \sim r^2, \quad u_3^H(r) \sim 2r^5. \quad (\text{A45})$$

For $r \geq R$ eqs. (A43) reduce to

$$\begin{aligned} \frac{d\chi_3}{dr} &= \frac{u_3}{r^4}, \\ \frac{du_3}{dr} &= \frac{10\chi_3 r^3}{(r-2M)} + \frac{u}{5} \frac{d}{dr} [4k_2 - \frac{6J^2}{r^4}]. \end{aligned} \quad (\text{A46})$$

The solution of this system is found as a linear combination of the solution $\chi_{3_{ext}}^H, u_{3_{ext}}^H$ of the homogenous system found by putting $k_2 = J = 0$ in (A46), and of a particular solution of (A46), $\chi_{3_{ext}}^P, u_{3_{ext}}^P$ which falls to infinity faster than r^{-5} . Both solutions have been calculated by making use of MAPLE.

The homogeneous system admits two solutions, which, for $r \rightarrow \infty$, behave as $\sim r^{-5}$ and $\sim r^2$. Since the metric must be asymptotically flat, we have excluded the latter.

Thus the general solution for $r \geq R$ is

$$\begin{aligned} \chi_{3_{ext}} &= D\chi_{3_{ext}}^H + \chi_{3_{ext}}^P, \\ u_{3_{ext}} &= Du_{3_{ext}}^H + u_{3_{ext}}^P, \end{aligned} \quad (\text{A47})$$

and consequently

$$w_{3_{ext}} = Dw_{3_{ext}}^H + w_{3_{ext}}^P \quad (\text{A48})$$

where

$$\begin{aligned} w_{3_{ext}}^H(r) &= \left(\frac{7}{64r^3 M^7} \right) \left[-120r^3 M^2 \ln\left(\frac{r}{r-2M}\right) \right. \\ &+ 150r^4 M \ln\left(\frac{r}{r-2M}\right) - 45r^5 \ln\left(\frac{r}{r-2M}\right) \\ &\left. + 20rM^4 + 60r^2 M^3 - 210r^3 M^2 + 90r^4 M + 8M^5 \right] \end{aligned} \quad (\text{A49})$$

and

$$\begin{aligned} w_{3_{ext}}^P(r) &= \left(\frac{J}{480r^7 M^9} \right) \left[(1152J^2 M^9 + 700r^5 J^2 M^4 \right. \\ &+ 2100r^6 J^2 M^3 - 7350r^7 J^2 M^2 + 3150r^8 J^2 M \\ &+ 280r^4 J^2 M^5 + 1152Kr^3 M^{10} + 64J^2 r M^8 - 320J^2 r^2 M^7 \\ &+ 10080KM^5 r^8 + 1088KM^8 r^5 + 1664KM^9 r^4 \\ &- 23520KM^6 r^7 + 6720KM^7 r^6 + 16800KM^5 r^8 \ln\left(\frac{r}{r-2M}\right) \\ &- 4200r^7 J^2 M^2 \ln\left(\frac{r}{r-2M}\right) + 5250r^8 J^2 M \ln\left(\frac{r}{r-2M}\right) \\ &- 5040KM^4 r^9 \ln\left(\frac{r}{r-2M}\right) - 13440KM^6 r^7 \ln\left(\frac{r}{r-2M}\right) \\ &+ 576KM^7 r^6 \ln\left(\frac{r}{r-2M}\right) - 960KM^8 r^5 \ln\left(\frac{r}{r-2M}\right) \\ &\left. - 384KM^9 r^4 \ln\left(\frac{r}{r-2M}\right) - 1575r^9 J^2 \ln\left(\frac{r}{r-2M}\right) \right]. \end{aligned} \quad (\text{A50})$$

The constants C and D are found by matching the interior and the exterior solutions at $r = R$.

-
- [1] J. B. Hartle, *Astrophys. J.* **150**, 1005, (1967).
[2] J. B. Hartle, *Astrophys. Space Sci.* **24**, 385, 1973.
[3] J. B. Hartle, K. S. Thorne, *Astrophys. J.* **153**, 807, (1968).
[4] S. Chandrasekhar, J. Miller, *Mon. Not. Roy. Astron. Soc.*, **167**, 63, (1974).
[5] F. Weber, N. K. Glendenning, Weigel M. K., *Astrophys. J.* **373**, 579, (1991).
[6] F. Weber, N. K. Glendenning, *Phys. Lett.* **B265**, 1, (1991).
[7] F. Weber, N. K. Glendenning, *Astrophys. J.* **390**, 541, (1992).
[8] J. M. Lattimer, M. Prakash, *Astrophys. J.* **550**, 426, (2001).
[9] E. Berti, F. White, A. Maniopoulou and M. Bruni, *Mon. Not. Roy. Astron. Soc.*, **358**, 923 (2005).
[10] N. Stergioulas, *Living Reviews of Relativity* 2003-3, (<http://www.livingreviews.org/>) 2003
[11] S. Bonazzola, E. Gourgoulhon, M. Salgado & J.A. Marck, *Astron. Astrophys.* **278**, 421, (1993)
[12] M. Salgado, S. Bonazzola, E. Gourgoulhon & P. Haensel, *Astron. Astrophys.* **291**, 155, (1994)
[13] G. B. Cook, S. L. Shapiro and S. A. Teukolsky, *Astrophys. J.* **424**, 823, (1994).
[14] E. Berti and N. Stergioulas, *Mon. Not. Roy. Astron. Soc.*, **350**, 1416, (2004).
[15] G. Baym, C. J. Pethick and P. Sutherland, *Astrophys. J.* **170**, 299, (1971).
[16] C. J. Pethick, B. G. Ravenhall and C. P. Lorenz *Nucl. Phys.* **A584**, 675, (1995).
[17] J. L. Friedmann, J. R. Ipser and L. Parker, *Astrophys. J.* **304**, 115, (1986).
[18] P. Haensel, J.L. Zdunik, *Nature* **340**, 617, (1989)
[19] C.W. Misner, K.S. Thorne and J.A. Wheeler, *Gravitation* (W.H.Freeman & Co., New York, 1973).
[20] R. B. Wiringa, V. Fiks and A. Fabrocini, *Phys. Rev. C* **38**, 1010, (1988).
[21] A. Akmal, V. R. Pandharipande, *Phys. Rev. C* **56**, 2261, (1997)
[22] A. Akmal, V. R. Pandharipande, D.G. Ravenhall *Phys. Rev. C* **58**, 1804, (1998)
[23] V. R. Pandharipande, D. Pines and A. R. Smith, *Astrophys. J.* **208**, 550, (1976).
[24] R.B. Wiringa, V.G.J. Stoks, R. Schiavilla, *Phys. Rev. C* **51**, 38, (1995)
[25] P.S. Pudliner, V.R. Pandharipande, J. Carlson, S.C. Pieper, R.B. Wiringa, *Phys. Rev. C* **56**, 1720, (1997)
[26] S.C. Pieper and R.B. Wiringa, *Ann. Rev. Nucl. Part. Sci.* **51**, 53, (2001)
[27] J.D. Walecka, *Ann. Phys.* **83**, 491, (1974)
[28] O. Benhar, V. Ferrari, L. Gualtieri, *Phys. Rev. D* **70**, 124015, (2004)
[29] S.E. Thorsett, D. Chakrabarty, *Astrophys. J.* **512**, 288, (1999)
[30] I. A. Morrison, T. W. Baumgarte, S. L. Shapiro and V.R. Pandharipande, *Astrophys. J. Suppl.* **617**, L135, (2004).